Heliyon 10 (2024) e32714

Contents lists available at ScienceDirect

Heliyon

journal homepage: www.cell.com/heliyon

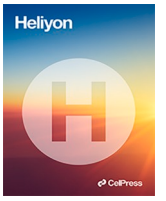

Research article

Exploring the multi-faceted potential: Synthesized ZnO nanostructure – Characterization, photocatalysis, and crucial biomedical applications

Maha M. Almoneef [a,*], Manal A. Awad [b,**], Haia H. Aldosari [c], Awatif A. Hendi [a], Horiah A. Aldehish [d], Nada M. Merghani [e], Saad G. Alshammari [f]

[a] Department of Physics, College of Science, Princess Nourah bint Abdulrahman University, P.O. Box 84428, Riyadh 11671, Saudi Arabia
[b] King Abdullah Institute for Nanotechnology, King Saud University, P.O. Box 2455, Riyadh 11451, Saudi Arabia
[c] Department of Physics, College of Science, Shaqra University, P.O. Box 5701, Shaqra 11961, Saudi Arabia
[d] Department of Botany and Microbiology, Faculty of Science, King Saud University, Riyadh, 11459, Saudi Arabia
[e] Central Research Laboratory, Vice Rectorate for Studies and Scientific Research, King Saud University, Riyadh 11451, Saudi Arabia
[f] Department of Chemistry, College of Science, King Saud University, P. O. 2455, Riyadh 11451, Saudi Arabia

ARTICLE INFO

Keywords:
ZnO
Synthesis
Medical applications
Cancer cell
Antibacterial

ABSTRACT

This research describes the methodology for synthesizing zinc oxide nanoparticles (ZnO-NPs). It demonstrates a unique, cost-effective, and non-toxic chemical technique for producing ZnO-NPs using the precipitation method with NaOH as reducing and capping agents. The formed nanoparticles have been characterized and analyzed using numerous techniques such as; Fluorescence emission spectroscopy (FL), X-ray diffraction (XRD), scanning electron microscopy (SEM), transmission electron microscopy (TEM), energy-dispersive X-ray Spectroscopy (EDX), ultraviolet–visible optical absorption (UV–Vis), Fourier transform infrared spectroscopy (FTIR), and Thermal gravimetric analysis (TGA). Also, the analytical technique X-ray diffraction studies has been used which showed that the ZnO-NPs had a Wurtzite hexagonal crystal structure with an average crystallite size of 34.27 nm. The form and the size of the synthesized ZnO-NPs have been seen in SEM and TEM photographs. Using J-image, particle size has been obtained at 13.33 nm, and the grain boundaries were all approximately spherical. Peaks in the FT-IR spectrum of the NPs indicate the presence of carboxylate (COO) and hydroxyl (O–H) functional groups. According to these findings, Zn interstitial defects are responsible for the 380 nm emission peak. Since EDX could not identify any impurities below the detection threshold, we may be sure that Zn and O are the principal components of the synthesized sample. ZnO-NPs cause an absorption band at 350.34 nm in the UV–Vis spectrum and a band gap of 3.24 eV. The catalytic activity of the synthesized ZnO nanoparticles (NPs) was evaluated by investigating their effectiveness in degrading crystal violet (CV) and methylene blue (MB) dyes, along with assessing the degradation rates. The results demonstrated a high degradation efficiency, with ZnO NPs achieving approximately 96.72 % degradation for CV and 97.169 % for MB dyes, underscoring their remarkable efficacy in the degradation process. As for antimicrobial activity assessment, the results revealed

* Corresponding author.
** Corresponding author.
E-mail addresses: mmalmoneef@pnu.edu.sa (M.M. Almoneef), mawad@ksu.edu.sa (M.A. Awad), haldossari@su.edu.sa (H.H. Aldosari), awatif.hindi@yahoo.com (A.A. Hendi), haldehish@KSU.EDU.SA (H.A. Aldehish), nmerghani@ksu.edu.sa (N.M. Merghani), Salshammari@ksu.edu.Sa (S.G. Alshammari).

https://doi.org/10.1016/j.heliyon.2024.e32714
Received 4 March 2024; Received in revised form 5 June 2024; Accepted 7 June 2024
Available online 13 June 2024

that the ZnO-NPs had negligible impact on Gram-negative bacteria, whereas they exhibited a discernible effect on Gram-positive bacteria. Additionally, it showed anti-cancer potential against colon (SW480), breast (MDA-231), and cervix (HELA) lines cells as seen by (MTT) assay. Hence, due to its simplified processes and cheaper chemicals, our synthesis technique may use in industrial settings for various applications.

1. Introduction

One material with enormous promise for the advancement and use of nanotechnology is zinc oxide (ZnO). ZnO is an ideal semiconductor due to its n-type direct bandgap of 3.37 eV at room temperature. The antibacterial and anticancer characteristics, as well as the availability and low cost of ZnO, have piqued the curiosity of scientists [1]. Traditional cancer treatments, which include chemotherapy, radiation, and surgery, have been around for a while. Cancer is characterized by the uncontrolled proliferation of malignant cells [2]. Zinc oxide nanoparticles (ZnO NPs) have gained significant traction in biological applications during the last twenty years owing to their low toxicity, cost-effectiveness, and superior biocompatibility. Particularly in the fields of antibacterial and anticancer treatment, ZnO NPs have shown great promise in biomedicine [3]. Among the many products of ZnO-NPs, which are synthesized through nanotechnology, are which have the powerful capacity to cause an excess of reactive oxygen species (ROS) to be produced, release zinc ions, and cause cell death. Zinc is also well recognized for maintaining the structural integrity of insulin. Therefore, ZnO NPs have also been successfully created for the treatment of diabetes. In addition, ZnO NPs are among the top contenders for bioimaging due to their exceptional luminous qualities [4–7].

The excellent absorption and scattering efficiency of ZnO-NPs for light in the UV and visible spectrum areas make them potential optoelectronics materials. Due to their high photoluminescence, ZnO-NPs are well-suited for emission display systems like T.V.s. The most promising options for photocatalytic degradation seem to be ZnO-NPs. Fabrics and wood may be shielded from UV rays with the help of ZnO-NPs [8]. Manufactured safely for the planet, ZnO-NPs effectively stop the spread of hazardous bacteria. ZnO-NPs, which are naturally antimicrobial, are utilized in food and container linings to prevent spoiling fish, peas, and corn. Some innovative biological uses for ZnO-NPs include medication delivery, antimicrobial treatment, and bioimaging [9].

Multiple investigations have consequently shown that ZnO-NPs kill cancer cells. The survival rate of cancer cells in MCF7, A549, HL60, and VERO cell lines has been studied at varying concentrations of ZnO. The results show that an increase in ZnO concentration considerably reduces cell viability of the cell above lines while causing only negligible damage to healthy cells [10].

However, there has been a surge in interest in ZnO's remarkable antibacterial activity, and research is underway to optimize the material by reducing its size, concentration, form, and imperfections while maintaining its potent nanobiological toxicity. Negative bacteria *E. coli* and other Gram-positive bacteria Research on the antimicrobial properties of ZnO nanoparticles often makes use of *Staphylococcus aureus* (*S. aureus*) as a model organism [11]. *Vibrio cholerae* and other Gram-negative bacteria live side by side with *Enterococcus faecalis* and Bacillus subtilis, two types of Gram-positive bacteria. Physically, it is unique from *Pseudomonas aeruginosa*, Proteus vulgaris, and P. vulgaris (ZnO). Moreover, probes are also performed [12,13]. ZnO-NPs made using environmentally friendly techniques were found to prevent the development of *Staphylococcus aureus*, *Escherichia coli*, and other bacteria at a higher rate than ZnO-NPs made using conventional methods [14]. However, researchers are still trying to pinpoint how ZnO-NPs achieve their antimicrobial effects. This study will discuss techniques for synthesizing zinc oxide and analyze the physical and optical characteristics of ZnO-NPs. After that, we will discuss the most critical medical findings and potential medicinal applications in anticancer and antibacterial activities.

In the literature review, various methods were found to have been developed for the production of ZnO nanopowders. These include sol-gel, microemulsion, spray pyrolysis, electrodeposition, ultrasonic, microwave-assisted techniques, chemical vapour deposition, hydrothermal, and precipitation. However, chemical synthesis has been frequently employed because of how easy it is to do and how cheap it is compared to the other methods. The chemical production of ZnO nanoparticles and their characterization by X-ray diffraction, scanning and transmission electron microscopy, selective area electron diffraction, ultraviolet–visible absorbance, and photoluminescence spectroscopy are detailed in this study.

2. Materials and experimental methods

2.1. Materials

The details of using materials for ZnO-NPs were clarified in Table 1.

Table 1
The materials information.

Chemicals	Chemical's structure	Manufacturer Company	Purity %
Sodium Hydroxide	NaOH	Loba Chemie, India	98 %
Zinc (II) chloride	$ZnCl_2$	Sigma-Aldrich, Germany	99.95 %
Distilled water	H_2O	VWR chemicals	–

2.2. Preparation of pure ZnO-NPs

Taking 1 M of zinc chloride ($ZnCl_2$) aqueous solution, stirring for half an hour, and then adding 2 M of sodium hydroxide (NaOH) aqueous solution dropwise to the previous solution is the chemical precipitation technique used to produce pure ZnO-NPs as shown in Fig. 1. After 3 h of stirring, the thick solution is filtered, cleaned with distilled water, and allowed to dry for 24 h. The resultant residue is ground and heated to 400 °C in a furnace.

2.3. Characterization of synthesized nanoparticles

2.3.1. Scanning electron microscopy (SEM) with energy dispersive X-ray analysis (EDX)

Compositional analysis of the synthesized ZnO-NPs was performed using the same scanning electron microscopy (SEM with EDXA, JSM-IT500HR-JEOL) that was used to examine the sample's morphology. The images are shown on a monitor. Present-day commercial SEMs often include cutting-edge data analysis software and an energy-dispersive X-ray Spectroscopy (EDX) instrument. The EDX also brought the advantages of employing software to assess the sample's composition to the table.

2.3.2. Transmission electron microscopy (TEM)

The main size of the ZnO-NPs was measured using transmission electron microscopy (TEM). The Zinclear_60CCT was dissolved in acetone to remove the ZnO-NPs, which were dried on a glass slide. The obtained powder was dissolved in ethanol at a concentration of 0.01–0.1 mM (using the unit cell of the ZnO crystal as a reference), and TEM (Philips CM10) images were taken.

2.3.3. X-ray diffraction (XRD)

Wide-angle X-ray diffraction (WAXD) experiments were conducted at room temperature using Siemens D5000 (Cu, GAXRD) equipment running at 40 kV. The CuK radiation, with a wavelength of 1.54178 A°, was the cause of the X-rays. Powder diffraction is often employed in this project because of the low difficulty of sample preparation and the speed and nondestructive nature of the tests. The powder diffraction pattern peaks assist in identifying materials quickly, while peak width or position variations help detect crystal size and texture.

2.3.4. Ultraviolet–visible spectroscopy (UV–Vis)

The UV–Vis spectrometer (PerkinElmer) was used to get readings of the absorption spectra of ZnO-NPs. The suspension was put in a high-quality U.V. quartz cuvette with a 2-mm passage to reduce scattering. The scattering means the route is substantially more significant than the pathway of the cuvette in the concentration range we studied; therefore, the scattering may be treated as a single event.

2.3.5. Fluorescence

A spectrophotometer from PerkinElmer (Waltham, MA, USA) was used to detect the fluorescence of ZnO-NPs in water. A quartz cell with a 1 cm route length was used to capture spectra ranging from 200 to 900 nm. The excitation wavelength of this experiment was 383 nm, and the emission slits were 1 nm wide.

2.3.6. Thermal gravimetric analysis (TGA)

The analysis was conducted using a PerkinElmer Pyris 1 TGA with a linear heating rate of 10 °C/min under a pure nitrogen environment at a flow rate of 60 ml/min. The temperature range varied from room temperature to 900 °C. Samples with an initial weight of 8–9 mg were used for the measurements, and the specimen was in solid form.

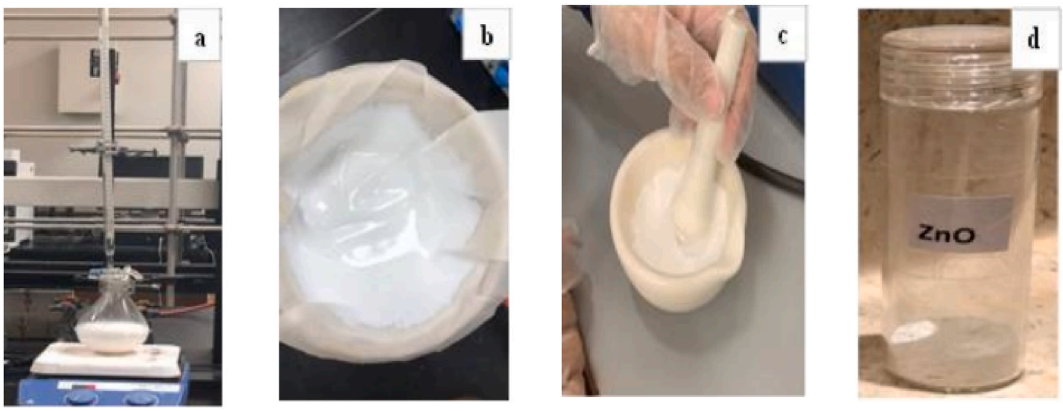

Fig. 1. Preparation steps of ZnO-NPs (a) stirring step, (b) filtering step, (c) grinding step, and (d) final product.

2.3.7. Fourier transform infrared spectroscopy (FTIR)

To obtain Fourier transform infrared (FTIR) analysis, the synthesized sample powder of about 2–3 mg was combined with about 0.5–1 g KBr, ground in a mortar to a fine, well-mixed powder, and then formed into a disk by exerting high pressure on a PerkinElmer Spectrum BX (PerkinElmer, Waltham, MA, USA).

2.4. Photocatalytic studies

ZnO-NPs had their photocatalytic potential measured by watching how quickly ponceau in a solution exposed to a visible light source deteriorates. The experimental flask was used to execute the photocatalytic process, which included adding 5 mg of NPs to 50 ml solutions of methylene blue (MB) and crystal violet (CV) dye at a concentration of 10 mg/L separately. Without NPs, the control group consists of dye solutions alone. To maintain the chemical component adsorption/desorption equilibrium on the catalyst surface, the reaction solution was first magnetically stirred in the dark for a few minutes before being exposed to UV radiation. The photocatalytic breakdown of the dyes was then accelerated by keeping the solution under a halogen light. A UV–Vis spectrophotometer was used every 3 h to test the colours' absorption.

$$DE\% = \frac{C_0 - C}{C_0} \times 100 \quad \text{Eq.1}$$

The degradation efficiency (DE%) is represented as a percentage, and the variables Co and C are the initial and final dye concentrations, respectively.

2.5. Biomedical assay

Cells from the colon (SW480), breast (MDA-231), and cervix (HELA) lines were planted at a density of 2×10^5 cells per well in 100 µl of optimal media in a 96-well plate for the MTT test. Trypan blue exclusion test (0.4 %) utilizing a cell counter established the total number of cells employed throughout all tests. After 24 h of rest, the cells were treated with varying concentrations of ZnO-NPs (3.125, 6.25, 12.5, 25, 50, and 100 µg/ml). After 24 h of treatment, cells were permitted to continue to increase.

Cell Titer 96® AQueous One Solution (Promega-G3582) should be used after a 48-h incubation period. To a 96-well assay plate containing samples in 100 µl of culture media, add 20 l of Cell Titer 96® AQueous One Solution Reagent. Then, place the plate in an incubator at 37 °C and 2 h of 5 % carbon dioxide humidity. This experiment aims to quantify the cellular breakdown of MTS that yields soluble formazan.

Finally, a 96-well plate reader (Molecular Devices -SPECTRA max- PLUS384) should be used to record the absorbance at 490 nm. Three independent experiments were conducted for each condition. Optical density values were adjusted to those of untreated cells as a baseline. Therefore, untreated cell viability measurements should equal 100 %, but treated cell viability values should be either less than or more than 100 %. For the math, we utilized this equation [15]:

$$\text{Cell viability } (\%) = \left[\frac{Total\ cells - viable\ cell}{Total\ Cells}\right] \times 100 \quad \text{Eq. 2}$$

To test the NPs' antibacterial properties, they were tested on autoclaved nutrient agar (14 g powder dissolved in 500 ml distilled water). Each Petri dish had 20 ml of agar placed into it, left to set for 15 min at room temperature, and then incubated overnight with human pathogens. *Staphylococcus aureus* (+ve), Staphylococcus epidermidis (+ve), Shigella sonnei (-ve), and *Salmonella enterica* (-ve), were collected at King Saud University's Botany and Microbiology lab. The disc diffusion technique was used to examine all bacterial species simultaneously. After filling the wells with the synthesized ZnO-NPs species employed in the research (1:3 µg and 2:7 µg,

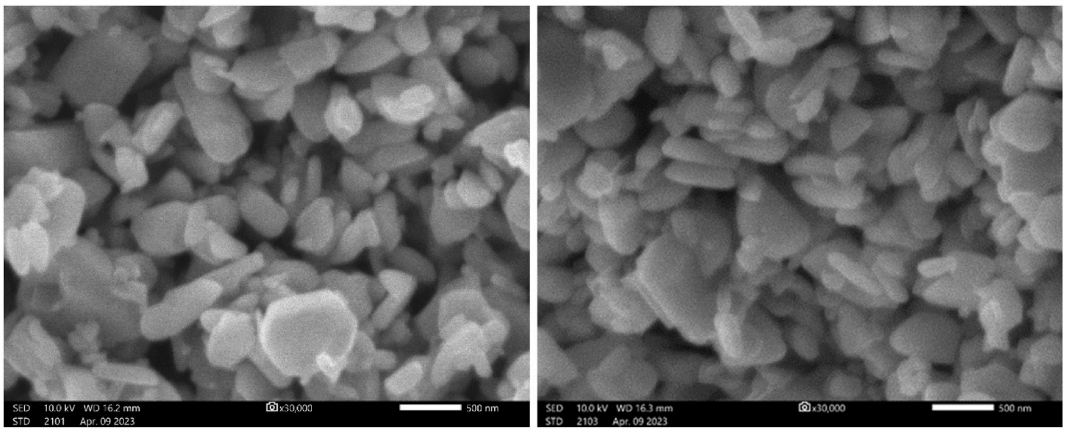

Fig. 2. SEM images of ZnO-NPs.

respectively), they were incubated at 37 °C for 24 h. It was determined how big the damping zone was.

3. Results and discussion

3.1. SEM and EDX study

The shape of the as-produced ZnO-NPs was examined at different magnifications in the Scanning Electron Microscopy (SEM) as shown in Fig. 2. The grain boundaries were all roughly spherical, and the particle sizes were easily discernible in a high-magnification SEM picture. Particles were found to be aggregated consistently, giving the impression of a literary-themed hierarchical sheet [16]. The EDX analysis of ZnO-NPs, as shown in Fig. 3, provides insight into the elemental makeup of the sputtered Zno-NPs' films. This data also allows us to determine the percentages of Zn and O by atomic and molecular weight. Since EDX could not identify any impurities below a certain threshold, we may conclude that Zn and O are the principal components of the sample [17,18].

3.2. TEM results

The ZnO particles are shown in TEM micrograph form in Fig. 4. This data points to the existence of ZnO-NPs in both quasi-spherical and irregular shapes. The sample's modest accumulation levels give it a structure similar to that of a cluster. Photos showing individual particles prove that the preparation procedure worked. ZnO-NPs were found to have particle sizes varied from 2.3 nm to 50.34 nm with a particle size distribution of 13.33 nm. According to the published research, these images corroborate the emergence of ZnO-NPs [19,20]. Images like these prove that nanoparticles are roughly spherical, with most showing facets. Selective electron diffraction (SAED) confirms nanocrystals' preferred orientation with a pattern of brilliant rings. The production of ZnO-NPs has also been shown in transmission electron microscopy images, which confirm the nanoparticles' hexagonal plane at various magnifications [21].

3.3. XRD study

A peak appears in the diffraction pattern when the strengths of all the diffracted atoms in a crystal are added together, as shown in Fig. 5. Since there are so many atoms in a bulk crystal, the total tends to converge, resulting in a delta function or a sharp peak. However, nanoparticles are constructed from tiny crystallites that contain a discrete number of atoms. The X-ray diffraction pattern for ZnO-NPs has prominent peaks at 2theta values of 31.73°, 34.37°, 36.21°, 47.47°, 56.55°, 62.77°, 66.31°, 67.87°, and 69.01°, corresponding to the planes (100), (002), (101), (102), (110), (103), (200), (112), and (201) [22]. An X-ray diffraction pattern of ZnO nanopowder is shown in Fig. 5. The processed material likely contains particles on the nanoscale, since the XRD peaks' lines have noticeably widened. Full width at half maximum (FWHM) data, peak intensity, location, and width were all computed from these XRD patterns. The diffraction peaks seen at 31.84°, 34.52°, 36.33°, 47.63°, 56.71°, 62.96°, 68.13°, and 69.18° are characteristic of the hexagonal wurtzite phase of zinc oxide, with lattice constants a = b = 0.281 nm and c = 0.521 nm (JCPDS card no. 00-036-1451) [23–25]. Furthermore, the absence of any XRD peaks other than those associated with ZnO verifies that the produced nanopowder is pure. The average crystallite size of the sample was determined to be 34.27 nm using the Debye-Scherrer formula [26]:

$$D = \frac{0.89\,\lambda}{\beta \cos\theta} \qquad \text{Eq. 5}$$

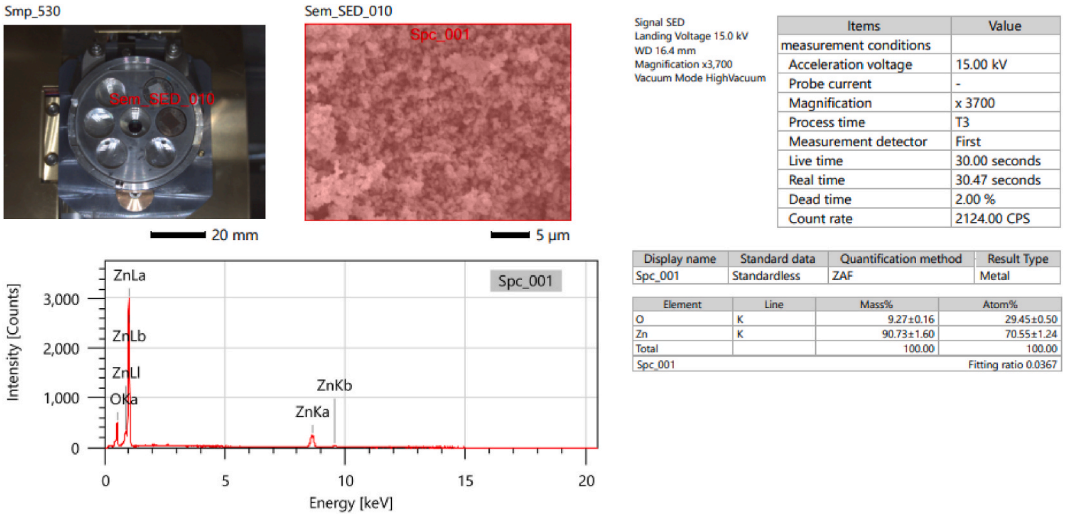

Fig. 3. EDX results and mapping of ZnO-NPs.

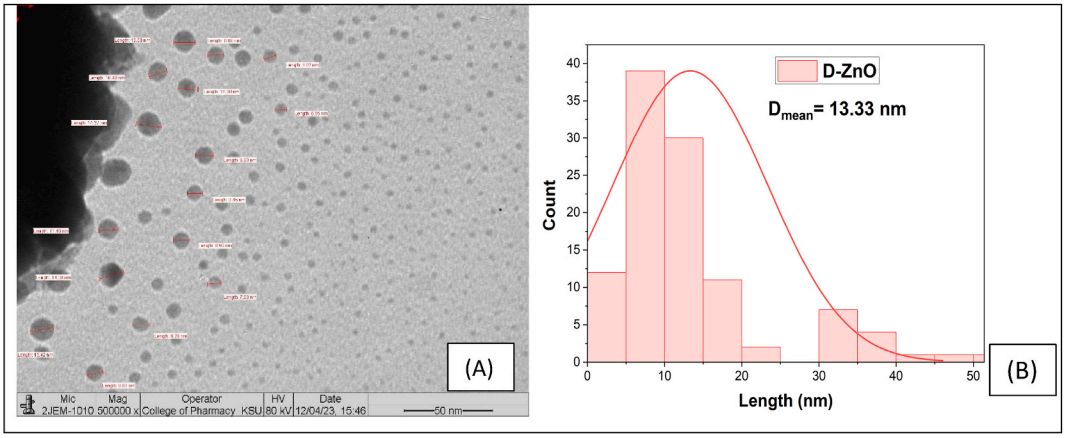

Fig. 4. TEM images of ZnO-NPs (A), the particle size distribution of ZnO-NPs (B).

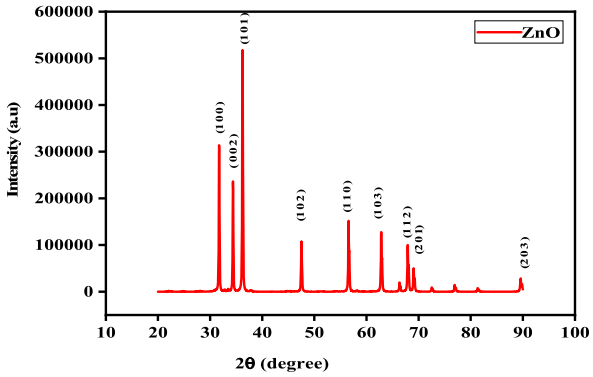

Fig. 5. XRD pattern of ZnO-NPs.

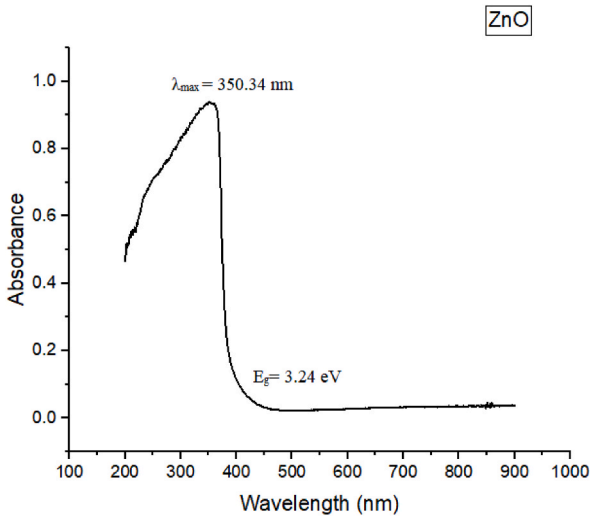

Fig. 6. UV–Vis absorption curve of ZnO-NPs.

where 0.89 is Scherrer's constant, λ is the X-ray wavelength, θ is the Bragg diffraction angle, and β is the full width at half maximum (FWHM) of the diffraction peaks.

3.4. UV–vis spectra

The UV–visible absorbance spectrum of ZnO-NPs in aqueous suspension is in Fig. 6 shown. At around 350.34 nm, there is a clearly visible absorption peak in the spectrum, which may be attributed to ZnO's natural bandgap absorption. This prominent peak demonstrates both the monodispersed nature of the nanoparticle distribution as well as the predominance of the nanoscale within the particle size distribution [27]. ZnO was the only peak in the spectrum, indicating that no further peaks were created during the synthesis. A significant decline follows a strong absorption band at about 350.34 nm. Significant acute absorption of ZnO also shows a little aggregation of the nanoparticles. Optical band gap can be found out using Tauc's equation [28]:

$$(ahv)m = A\ (hv\ -\ Eg) \quad \text{Eq. 6}$$

Where m is a parameter which is 2 for a direct transition, (hv) is the incident photon energy in this instance, (A) is the pre-factor constant, which is independent of photon energy for this transition and the absorption coefficient (α) is calculated using absorbance information. Our computation yields an optical band gap of 3.24 eV [29]. The overall properties of a material are significantly affected by the size of the nanoparticles. Thus, in order to comprehend the properties of semiconducting nanoparticles, it is essential to investigate their size evolution. Using UV–visible absorption spectroscopy, researchers often examine the optical properties of nanoparticles [30].

3.5. FT-IR analysis

The unique functional group linked to the synthesized zinc oxide nanoparticles was located by means of FT-IR analysis (Fig. 7). Carboxylate (COO) and hydroxyl (O–H) impurities are indicated as peaks at 1000-4000 cm^{-1} in the FTIR spectra of the NPs. Typical of the zinc oxide nanoparticles produced in this research, the peaks indicate a functional group [31]. The presence of water molecules on the surface of ZnO-NPs is indicated by a broad band at around 3500 cm^{-1} which corresponds to the O–H stretching mode of the hydroxyl group. The samples' absorbance maxima at 1630 and 1396 cm^{-1} are caused by the symmetric and asymmetric stretching carboxylates that are attached to the ZnO-NPs during manufacturing, which is in agreement with [32]. The plasma species containing reactive carbon are likely the carboxylate source during ZnO-NPs production. The number of carboxylate groups in a sample decreases as nanoparticle size increases. According to Ref. [33], the absorption peak at 440 cm^{-1} is caused by the vibration mode of metal-oxygen (ZnO stretching vibrations). This finding proves that ZnO nanoparticles were successfully manufactured.

3.6. Fluorescence spectrum

The fluorescence spectrum obtained from a 383 nm-excited aqueous solution of ZnO nanoparticles is shown in Fig. 8. The emission peaks of ZnO, which typically range from 380 to 750 nm, are all visible in the spectrum. The results of this investigation indicate that the emission peak at 380 nm is caused by the creation of Zn interstitial defects and that the strong emission at 750 nm, which may have originated from antisite defects, is caused by the generation of oxygen vacancy defects. It is well recognized that the main causes of

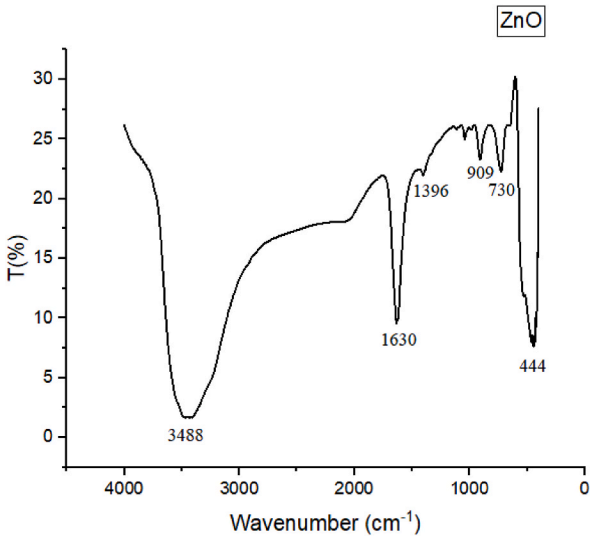

Fig. 7. FT-IR spectrum of the ZnO-NPs.

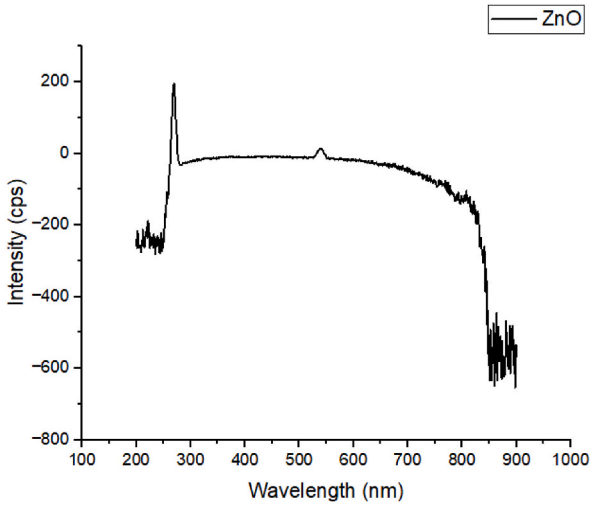

Fig. 8. Synthesized ZnO nanoparticles' fluorescence emission spectrum.

visible luminescence are faults in emission at deep levels, including oxygen vacancies and zinc interstitials [34]. When a photo-generated hole combines with the defect's single ionized charge state, it creates a single ionized oxygen vacancy, which in turn induces emission in ZnO. This is the result of recombining the defect's single ionized charge state with a photo-generated hole [35].

3.7. Thermal stability

The TGA thermogram for ZnO-NPs is shown in Fig. 9. It should be noted that the observed TGA data of ZnO-NPs show that the weight loss proceeds in successive stages with increasing temperature. The first step is in the range of 150 °C to about 200 °C, demonstrating the dehydration of surface-adsorbed water. The second step, which is a major weightlessness tape, occurs in the range of 200 °C to about 350 °C, indicating the loss of OH^- and CO_3^{2-}, with additional weight loss observed up to a temperature of 900 °C, as can be seen from the TGA curve, the precursor can be completely decomposed to ZnO after annealing at ~900 °C.

3.8. Photocatalytic studies

By degrading organic MB and CV dyes in a water-based solution exposed to a UV light source lamp, the photocatalytic degradation efficiency of pure ZnO NPs was examined. The proportion of dye degradation was evaluated using a UV–Vis spectrophotometer. Dye colours shift and absorb light differently as time passes (Fig. 10-A). While the maximum degradation of ZnO-NPs against CV was determined to be 96.72 % after 24 h, the maximum degradation of M.B. dyes was 97.169 % (Fig. 10-B). Intense light causes

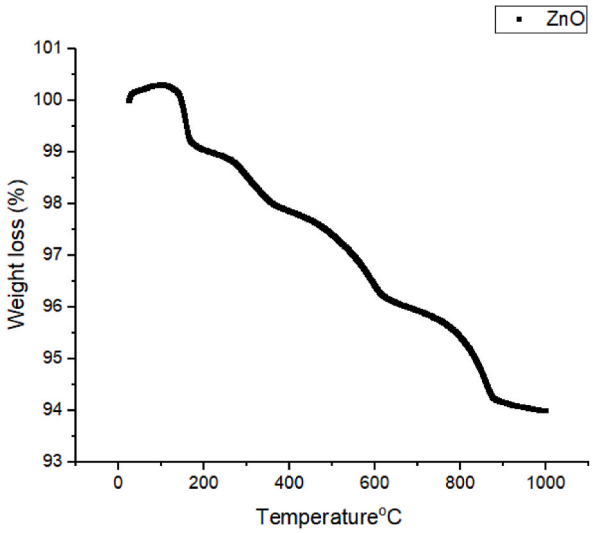

Fig. 9. TGA analysis of the synthesized ZnO NPs.

semiconductor electrons to escape, creating positively charged holes in ZnO, which speeds up the photocatalytic activity of ZnO nanoparticles [36]. The photoelectrochemical mechanism of ZnO-NPs involves reduction reactions caused by ZnO's electrons and oxidation events caused by its holes migrating to its surface. When electrons migrate to the adsorbed O_2 via the conduction band of ZnO, superoxide radicals (radical dotO_2) are formed. O.H. radicals are produced when the radical dotO_2 combines with the trapped electrons to form H_2O [37]. Therefore, it is believed that the high photocatalytic degradation of dyes is mainly due to redox reactions and hydroxyl radicals in ZnO-NPs. Data depicted in Fig. 10-C demonstrates that the degradation rate of dyes increases with progression when they are exposed to halogen light at various time intervals. Previous investigations produced the same findings. The production of holes, which are positively charged, and electrons, which are negatively charged, happens when nanoparticles absorb light of a specific wavelength, which excites the particle and causes an electron shuffle from the valence band to the conduction band [38]. The hydroxyl radical (radical dotOH) production happens when water molecules in the vicinity react with positively charged holes. In contrast, the radical anion (radical dotO_2^-) develops when molecular oxygen reacts with negatively charged electrons. In most cases, the photocatalytic activity of organic dyes is attributed to the hydroxyl radicals (radical dotOH) and the reactive oxygen anion (radical dot O_2^-) (as shown in Fig. 15 [39].

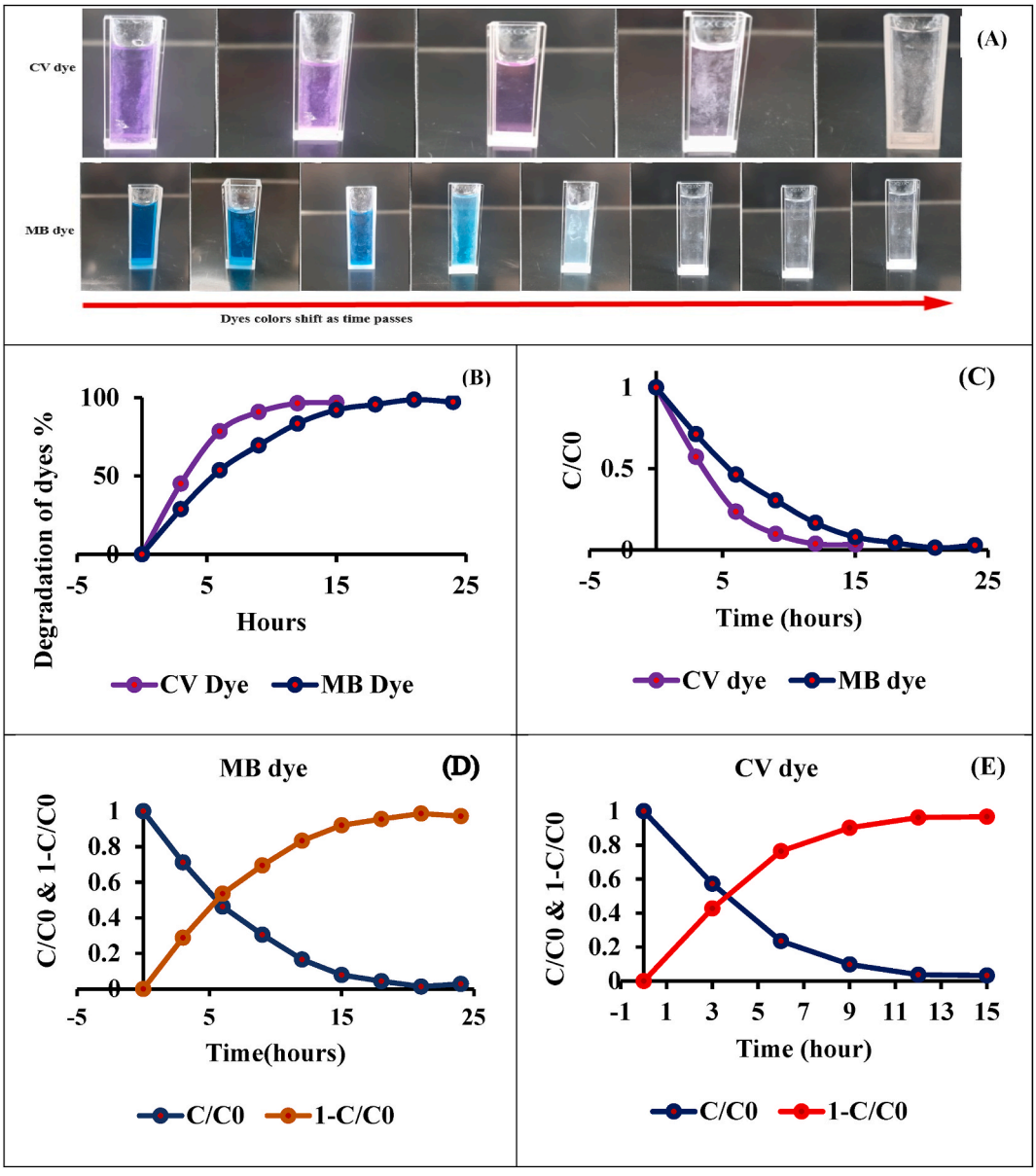

Fig. 10. The colours of dyes undergo a shift over time (A), Photocatalytic degradation of dyes (B), Degradation % of ZnO-NPs (C), Catalytic efficiency of NPs against dyes (D), The half-life period of dyes treated using ZnO-NPs (E). (For interpretation of the references to colour in this figure legend, the reader is referred to the Web version of this article.)

The effectiveness of catalysts was assessed by calculating the half-life of dyes by squaring the intersection of the curves representing the concentration of dye (C/C0) and the degradation rate (1-C/C0). Fig. 10-(D, E) shows the half-life of ZnO-NPs; for M.B. dyes, it was estimated to be about 6 h, while for CV dyes, it was around 3 h [40]. The photocatalytic utilization of zinc oxide nanoparticles made from bio-waste and other natural resources to clean up dye-contaminated water, while also reducing environmental impact.

When do comparing our results with similar studies involving ZnONPs-based photocatalysts synthesized through various methods and documented in the some previous literatures, it's noteworthy that our findings demonstrate a higher degradation percentage compared to other reported cases, as highlighted in Table 2.

3.9. Biomedical assay

As the concentration (3.125, 6.25, 12.5, 25, 50, and 100 μg/ml) of ZnO-NPs increased, the cancer rate of cells dropped. According to Figs. 11–13, the cell viability was at its lowest at concentrations of 50–100 μg/ml of ZnO. The inhibitory effect of the NPs has been observed in vitro on colon (SW480), breast (MDA-231), and cervix (HELA) cancer cells using the MTT assay. Lower concentrations of the NPs (3.125–12.5 μg/ml) slightly reduced cell viability in all cells (Figs. 11–13). At higher concentrations (25–100 μg/ml) of NPs, we decreased cell viability by more than 50 % in all cells. The inhibition of cell viability is concentration dependent in all cells. Both plant extracts and synthesized nanoparticles showed more toxicity on MDA-231 and HELA cells than on SW480 cells (Figs. 11–13; respectively).

Numerous studies investigating the effects of ZnO nanoparticles on various cell lines align with the current research findings. For instance, Selvakumari et al. demonstrated the antitumor potential of ZnO nanoparticles on breast cell lines, revealing that 31 μg of these nanoparticles eliminated 50 % of tumour cells [47]. Another study showcased the notable antitumor impact of ZnO nanoparticles on glioma (T98G) cells without causing cytotoxicity in HEK293 cells. This study also highlighted the genotoxic effects of ZnO nanoparticles inducing apoptosis in tumour cells, particularly activating the ROS pathway. In a separate investigation by Wahab et al. the treatment of HepG2 liver cancer and breast cancer cells with ZnO nanoparticles at 25 μg/ml induced apoptosis, reducing viable cells to below 10 %, and at 70 μg/ml, it decreased SW40 cell viability by 50 % [48]. Furthermore, Boskabadi, S. H. reported on both dose-dependent and time-dependent assessments of ZnO nanoparticle cytotoxicity, revealing different IC50 values across treated cell lines. The IC50 results demonstrated that while ZnO nanoparticles exhibited toxicity towards cancer cells, they remained safe and non-toxic for normal cell types. These outcomes highlight a significant inhibition of cancer cell proliferation based on ZnO nanoparticle treatment doses. Moreover, higher doses of ZnO nanoparticles and longer incubation times (>48 h) notably decreased cancer cell survival [49].

While the precise mechanisms responsible for the cytotoxic effects of ZnO-NPs are still under investigation, there is a widely accepted belief that the generation of reactive oxygen species (ROS) plays a pivotal role. Hence, it is speculated that the principal reason behind the cytotoxicity of ZnO-NPs in cancer cells lies in their distinct ability to induce oxidative stress. This characteristic trait is attributed to their semiconductor behaviour. ZnO-NPs, upon surpassing the antioxidant capacity of the target cell, escalate ROS production, instigating oxidative stress that ultimately leads to cell death [50,51]. The absorption of ZnO nanoparticles through the respiratory system and gastrointestinal wall can trigger the generation of free oxygen radicals through the ROS pathway, aiding in the elimination of tumour cells. Studies have shown that the presence of these nanoparticles over tumour cells activates the synthesis of the iNOS enzyme, leading to the production of nitric oxide, interleukin 1 (IL-1), interferons, and tumour necrosis factor, all contributing to inflammation. These factors stimulate the iNOS enzyme within tumour cells, creating a positive feedback loop that generates more nitric oxide. nitric oxide generated by cells follows two paths: first, inducing apoptosis by affecting cell DNA and facilitating deeper penetration of ZnO nanoparticles, causing cell damage through membrane lipid peroxidation (Fig. 15). Second, nitric oxide decreases the proliferation and potency of lymphocytes responsible for the anti-inflammatory response, thereby impeding the formation of anti-inflammatory factors and enhancing apoptosis signals. Consequently, nitric oxide inflicts more damage on tumour tissue and hinders the activity of anti-inflammatory lymphocytes [52].

Table .3 displays the impact of synthesized ZnO-NPs on bacterial reduction, whereas Fig. 14 illustrates *Staphylococcus epidermidis*. The visual elements within the image include the antibiotic positioned at the top, flanked by ZnO on the left and right sides. The findings revealed that the ZnO nanoparticles, when prepared, exhibited no discernible impact on Gram-negative bacteria such as *S. enterica* and *S. sonnei*. However, they demonstrated an effect on Gram-positive bacteria, notably *S. aureus* and *S. epidermidis*. Conversely, the antibiotic displayed a pronounced effect on all types of bacteria, irrespective of their Gram classification.

Numerous studies have documented the antibacterial activities of zinc oxide nanoparticles (ZnO- NPs), emphasizing that their efficacy varies based on the sensitivity of the targeted microorganism [53]. *Shinde* et al. [54] conducted a study on ZnO microspheres against Gram-positive (*S. aureus*) and Gram-negative (*E. coli*), suggesting differences in susceptibility based on the bacteria's cell wall structure. Gram-positive bacteria have a thick peptidoglycan layer, providing a physical barrier, while Gram-negative bacteria have a thinner peptidoglycan layer and an external membrane with lipopolysaccharides. NPs, with various sizes, can easily pass through the peptidoglycan layer, causing damage. ZnO-NPs interact with carboxylic acid and amino groups in the peptidoglycan layer, inhibiting cellular processes. The thinner peptidoglycan layer in Gram-negative bacteria makes the cell membrane more susceptible to rupture. *Tayel* et al.*'s* study further highlighted that Gram-positive bacteria are more susceptible to ZnO-NPs attack than Gram-negative bacteria. Reddy et al. observed that the minimum inhibitory concentration of ZnO-NPs was lower for Gram-positive (1 mg/ml) compared to Gram-negative (3.4 mg/ml) [55]. This suggests that higher concentrations of ZnO-NPs are needed to inhibit Gram-negative bacteria, potentially due to the protective role of lipopolysaccharides in their cell wall (Fig. 15). Similar findings by d'Agua et al. using textiles containing ZnO-NPs indicated greater sensitivity of Gram-positive bacteria to ZnO than Gram-negative bacteria in terms of antibacterial activity [56]. In summary, while nanoparticle morphology is a crucial parameter, the antimicrobial mechanisms of ZnO-NPs are

Table 2
Compares the efficacy of the current synthesized ZnO-NPs with values reported in the previous literatures for ZnONPs as photocatalysts.

Methods of Synthesis of ZnONPs	Dye	Source of Light	Degradation Percentage (%) of Dye
Precipitation	MB	UV lamp	81 % [41]
sol-gel	Coomassie Brilliant Blue R-250, Acid Blue, and Congo red	UV lamp	70 %, 73 %, and 88 %; respectively [42]
Co-Precipitation method	Rhodamine	UV	88 % [43]
Hydrothermal Method	MB	UV irradiation	39.56 % [44]
microwave assisted method	MB	Sun light	80 % [45]
Green synthesis method	tartrazine yellow	Visible light	76.1 % [46]
Precipitation	MB, and CV	ultraviolet light	97.169 % and 96.72 % [current study]

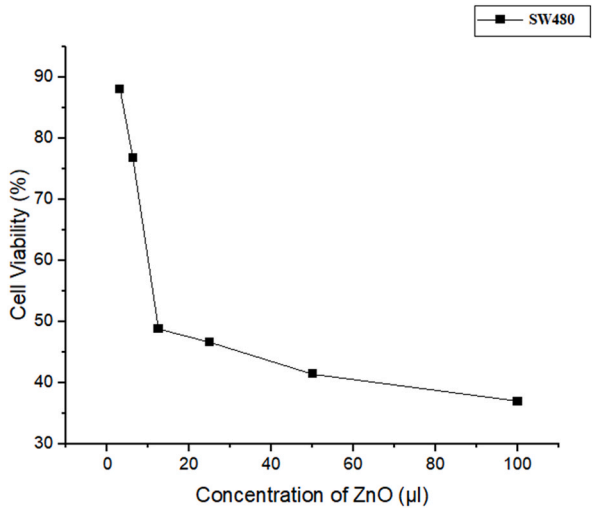

Fig. 11. The cell viability percentages of SW480 with different concentrations of ZnO-NPs.

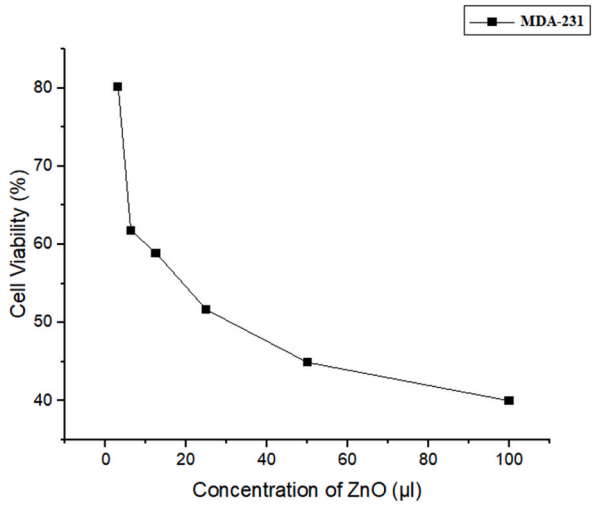

Fig. 12. The cell viability percentages of MDA-231 with different concentrations of ZnO-NPs.

primarily size-dependent. Smaller-sized ZnO-NPs tend to exhibit optimized antimicrobial activity. Additionally, the surface properties of nanomaterials play a significant role in influencing interactions with cells and can potentially interfere with the antimicrobial effects of ZnO-NPs [57].

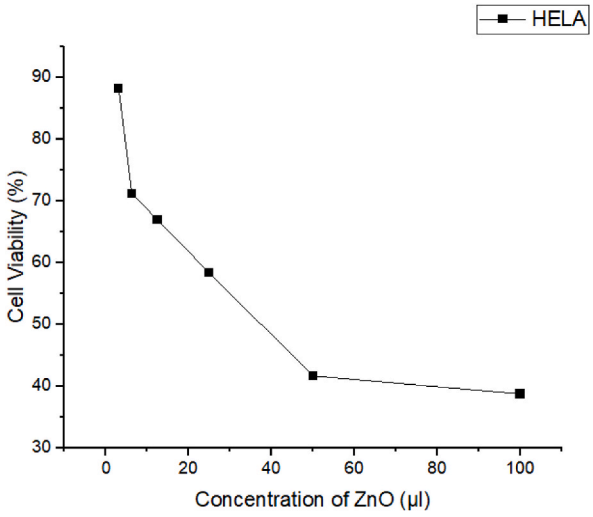

Fig. 13. The cell viability percentages of HeLa with different concentrations of ZnO-NPs.

Table 3
The bacterial reduction as an effect of ZnO-NPs.

Bectria	Sample ID	Zones Inhibition (mm)
Salmonella enterica (-ev)	Antibiotic	2.0
	ZnO1	0.0
	ZnO2	0.0
Shigella sonnei (-ev)	Antibiotic	2.2
	ZnO1	0.0
	ZnO2	0.0
Staphylococcus aureus (+ev)	Antibiotic	1.9
	ZnO1	0.6
	ZnO2	0.8
Staphylococcus epidermidis (+ev)	Antibiotic	2.5
	ZnO1	0.8
	ZnO2	1.0

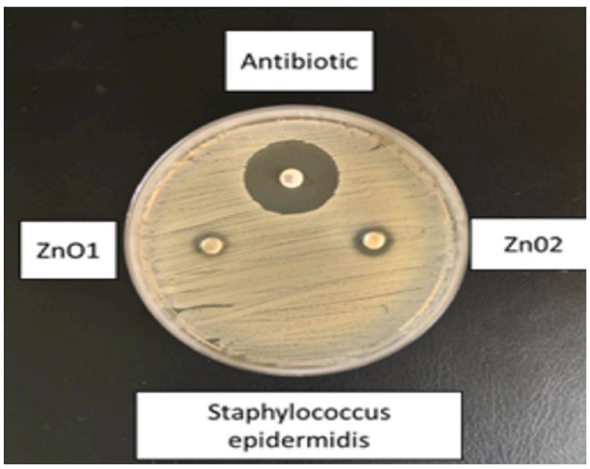

Fig. 14. The antibacterial activity of ZnO-NPs against *Staphylococcus epidermidis*.

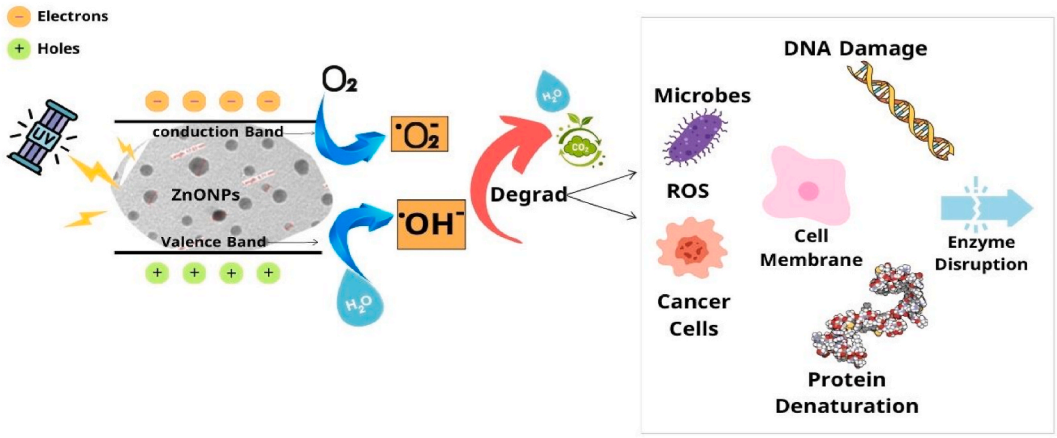

Fig. 15. Understanding the photocatalytic mechanisms driving antimicrobial and anticancer properties of ZnO nanoparticles.

4. Conclusion

A non-toxic and economical chemical approach was employed to efficiently synthesize zinc oxide nanoparticles, utilizing the precipitation process with NaOH acting as both reducing and capping agents. XRD analysis unveiled that the ZnO-NPs exhibited an average crystallite size of approximately 34.27 nm and adopted a Wurtzite hexagonal structure. The presence of ZnO nanoparticles induced the absorption band at 350.34 nm in the UV–vis absorption spectrum. Notably, no impurities were detected within the EDX detection range, confirming Zn and O as the primary components of the synthesized sample. TEM analysis provided visual evidence of the quasi-spherical and irregular shapes of the zinc oxide nanoparticles, with minimal agglomeration resulting in a clustered appearance. Functional group analysis via FTIR spectroscopy further validated the successful synthesis, with vibrational phonon peaks in the FTIR spectrum corroborating the presence of ZnO-NPs. A UV–Vis spectrophotometer was employed to analyze the optical characteristics of synthesized ZnO-NPs. Results unveiled a broad green emission band linked to oxygen vacancies and a distinct ultraviolet band indicative of excitonic emission near the band gap ($\lambda exc = 350.34$ nm). The photocatalytic performance of the ZnO-NPs was evaluated through the degradation of dyes. Impressively, they exhibited approximately 96.72 % degradation for CV and 97.169 % for MB dyes, highlighting their exceptional efficacy in the degradation process. Moreover, the synthesized ZnO nanoparticles exhibited promising inhibitory effects on the proliferation of cancerous and bacterial cells at specific doses, suggesting their potential integration into medical devices for antibacterial and anticancer therapies. The finding of this research underscores the promising potential of ZnO-NPs as a viable candidate for various industrial applications, as well as biomedical applications.

CRediT authorship contribution statement

Maha M. Almoneef: Writing – review & editing, Visualization, Supervision, Project administration, Methodology, Investigation, Funding acquisition. **Manal A. Awad:** Writing – original draft, Validation, Methodology, Data curation, Conceptualization. **Haia H. Aldosari:** Writing – original draft, Methodology, Data curation. **Awatif A. Hendi:** Validation. **Horiah A. Aldehish:** Formal analysis, Data curation. **Nada M. Merghani:** Formal analysis, Data curation. **Saad G. Alshammari:** Formal analysis, Data curation.

Declaration of competing interest

The authors declare that they have no known competing financial interests or personal relationships that could have appeared to influence the work reported in this paper.

Acknowledgement

This research was funded by Princess Nourah bint Abdulrahman University Researchers Supporting Project number (PNURSP2024R56), Princess Nourah bint Abdulrahman University, Riyadh, Saudi Arabia.

References

[1] P. Sivakumar, M. Lee, Y.S. Kim, M.S. Shim, Photo-triggered antibacterial and anticancer activities of zinc oxide nanoparticles, J. Mater. Chem. B 6 (30) (2018) 4852–4871.
[2] A. Hussain, M. Oves, M.F. Alajmi, I. Hussain, S. Amir, J. Ahmed, M.T. Rehman, H.R. El-Seedi, I. Ali, Biogenesis of ZnO nanoparticles using Pandanus odorifer leaf extract: anticancer and antimicrobial activities, RSC Adv. 9 (27) (2019) 15357–15369.
[3] H. Sharma, K. Kumar, C. Choudhary, P.K. Mishra, B. Vaidya, Development and characterization of metal oxide nanoparticles for the delivery of anticancer drugs, Artif. Cell Nanomed. Biotechnol. 44 (2) (2016) 672–679.
[4] J. Malik, ZnO Nanoparticles: Growth, Properties, and Applications, 2015.

[5] M. Zarrabi, M. Haghighi, R. Alizadeh, S. Mahboob, Solar-light-driven photodegradation of organic dyes on sono-dispersed ZnO nanoparticles over graphene oxide: sono vs. conventional catalyst design, Sep. Purif. Technol. 211 (2019) 738–752.
[6] M. Pudukudy, Z. Yaakob, Facile synthesis of quasi spherical ZnO nanoparticles with excellent photocatalytic activity, J. Cluster Sci. 26 (2015) 1187–1201.
[7] P. Sadhukhan, M. Kundu, S. Rana, R. Kumar, J. Das, P.C. Sil, Microwave-induced synthesis of ZnO nanorods and their efficacy as a drug carrier with profound anticancer and antibacterial properties, Toxicol Rep 6 (2019) 176–185.
[8] Y. Zhang, T. R Nayak, H. Hong, W. Cai, Biomedical applications of zinc oxide nanomaterials, Curr. Mol. Med. 13 (10) (2013) 1633–1645.
[9] M. Martínez-Carmona, Y. Gun'Ko, M. Vallet-Regí, ZnO nanostructures for drug delivery and theranostic applications, Nanomaterials 8 (4) (2018) 268.
[10] M. Premanathan, K. Karthikeyan, K. Jeyasubramanian, G. Manivannan, The selective toxicity of ZnO nanoparticles toward Gram-positive bacteria and cancer cells by apoptosis through lipid peroxidation, Nanomed. Nanotechnol. Biol. Med. 7 (2) (2011) 184–192.
[11] F. Islam, S. Shohag, M.J. Uddin, M.R. Islam, M.H. Nafady, A. Akter, S. Mitra, A. Roy, T.B. Emran, S. Cavalu, I am exploring the journey of zinc oxide nanoparticles (ZnO-NPs) toward biomedical applications—materials 15 (6) (2022) 2160.
[12] D. Selvakumari, R. Deepa, V. Mahalakshmi, P. Subhashini, N. Lakshminarayan, Anti-cancer activity of ZnO nanoparticles on MCF7 (breast cancer cell) and A549 (lung cancer cell), ARPN J. Eng. Appl. Sci. 10 (12) (2015) 5418–5421.
[13] Y. Li, C. Zhang, L. Liu, Y. Gong, Y. Xie, Y. Cao, The effects of baicalein or baicalin on the colloidal stability of ZnO nanoparticles (NPs) and toxicity of NPs to Caco-2 cells, Toxicol. Mech. Methods 28 (3) (2018) 167–176.
[14] S. Bagheri, K.G. Chandrappa, S.B.A. Hamid, Facile synthesis of nanosized ZnO by direct precipitation method, Der Pharma Chem. 5 (3) (2013) 265–270.
[15] S. Kamiloglu, G. Sari, T. Ozdal, E. Capanoglu, Guidelines for cell viability assays, Food Frontiers 1 (2020) 332–349.
[16] E. Albalghiti, L.M. Stabryla, L.M. Gilbertson, J.B. Zimmerman, Towards resolution of antibacterial mechanisms in metal and metal oxide nanomaterials: a meta-analysis of the influence of study design on mechanistic conclusions, Environ. Sci.: Nano 8 (1) (2021) 37–66.
[17] K.M. Reddy, K. Feris, J. Bell, D.G. Wingett, C. Hanley, A. Punnoose, Selective toxicity of zinc oxide nanoparticles to prokaryotic and eukaryotic systems, Appl. Phys. Lett. 90 (21) (2007).
[18] Y.H. Hsueh, W.J. Ke, C.T. Hsieh, K.S. Lin, D.Y. Tzou, C.L. Chiang, ZnO nanoparticles affect Bacillus subtilis cell growth and biofilm formation, PLoS One 10 (6) (2015) e0128457.
[19] M. Divya, B. Vaseeharan, M. Abinaya, S. Vijayakumar, M. Govindarajan, N.S. Alharbi, S. Kadaikunnan, J.M. Khaled, G. Benelli, Biopolymer gelatin-coated zinc oxide nanoparticles showed high antibacterial, antibiofilm and anti-angiogenic activity, J. Photochem. Photobiol. B Biol. 178 (2018) 211–218.
[20] M. Divya, B. Vaseeharan, M. Abinaya, S. Vijayakumar, M. Govindarajan, N.S. Alharbi, S. Kadaikunnan, J.M. Khaled, G. Benelli, Biopolymer gelatin-coated zinc oxide nanoparticles showed high antibacterial, antibiofilm and anti-angiogenic activity, J. Photochem. Photobiol. B Biol. 178 (2018) 211–218.
[21] N. Promsawat, W. Wichaiwong, P. Pimpawat, K. Changsarn, K. Phimol, M. Promsawat, P. Janphuang, A study of flexible piezoelectric generators by sputtering ZnO thin film on PET substrate, Integrated Ferroelectrics Int. J. 195 (1) (2019) 220–229.
[22] M.I. Khalil, M.M. Al-Qunaibit, A.M. Al-Zahem, J.P. Labis, Synthesis and characterization of ZnO nanoparticles by thermal decomposition of a curcumin zinc complex, Arab. J. Chem. 7 (6) (2014) 1178–1184.
[23] A. Bouzidi, K. Omri, H. Jilani, S. Yahia, Effect of the different concentrations of ZnO:Mn incorporation on the microstructure and dielectric properties of epoxy nanocomposites, J. Mater. Sci. Mater. Electron. 29 (7) (2018) 5908–5917.
[24] C. Mahendra, M. Murali, G. Manasa, P. Ponnamma, M.R. Abhilash, T.R. Lakshmeesha, A. Satish, K.N. Amruthesh, M.S. Sudarshana, Antibacterial and antimitotic potential of bio-fabricated zinc oxide nanoparticles of Cochlospermum religiosum (L.), Microb. Pathog. 110 (2017) 620–629.
[25] B.N. Singh, A.K.S. Rawat, W. Khan, A.H. Naqvi, B.R. Singh, Biosynthesis of stable antioxidant ZnO nanoparticles by Pseudomonas aeruginosa rhamnolipids, PLoS One 9 (9) (2014) e106937.
[26] N. Vijayakumar, V.K. Bhuvaneshwari, G.K. Ayyadurai, R. Jayaprakash, K. Gopinath, M. Nicoletti, S. Alarifi, M. Govindarajan, Green synthesis of zinc oxide nanoparticles using Anoectochilus elatus and their biomedical applications, Saudi J. Biol. Sci. 29 (4) (2022) 2270–2279.
[27] N. Promsawat, W. Wichaiwong, P. Pimpawat, K. Changsarn, K. Phimol, M. Promsawat, P. Janphuang, A study of flexible piezoelectric generators by sputtering ZnO thin film on PET substrate, Integrated Ferroelectrics Int. J. 195 (1) (2019) 220–229.
[28] K. Mubeen, et al., Band structure tuning of ZnO/CuO composites for enhanced photocatalytic activity, J. Saudi Chem. Soc. 27 (3) (2023) 101639–102023, https://doi.org/10.1016/j.jscs.2023.101639.
[29] A.C. Mohan, B.J.P.T. Renjanadevi, Preparation of zinc oxide nanoparticles and their characterization using scanning electron microscopy (SEM) and X-ray diffraction (XRD), Procedia Technology 24 (2016) 761–766.
[30] S. Sharma, K.N. Uttam, Rapid analyses of the stress of copper oxide nanoparticles on wheat plants at an early stage by laser-induced fluorescence and attenuated total reflectance Fourier transform infrared spectroscopy, Vib. Spectrosc. 92 (2017) 135–150.
[31] J. Zvezdanović, D. Marković, Bleaching of chlorophylls by U.V. irradiation in vitro: the effects on chlorophyll organization in acetone and n-hexane, J. Serb. Chem. Soc. 73 (3) (2008) 271–282.
[32] S. Getie, A. Belay, A.R. Chandra Reddy, Z. Belay, Synthesis and characterizations of zinc oxide nanoparticles for antibacterial applications, J. Nanomed. Nanotechnol. S 8 (4) (2017).
[33] P. Saravanan, K. Jayamoorthy, S.A. Kumar, Switch-On fluorescence and photoinduced electron transfer of 3-aminopropyltriethoxysilane to ZnO: dual applications in sensors and antibacterial activity, Sensor. Actuator. B Chem. 221 (2015) 784–791.
[34] K.R. Shin, S.I. Yoon, Y.G. Ko, D.H. Shin, Deposition of hydroxyl-apatite on titanium subjected to electrochemical plasma coating, Electrochim. Acta 109 (2013) 173–180.
[35] A. Hussain, M. Oves, M.F. Alajmi, I. Hussain, S. Amir, J. Ahmed, M.T. Rehman, H.R. El-Seedi, I. Ali, Biogenesis of ZnO nanoparticles using Pandanus odorifer leaf extract: anticancer and antimicrobial activities, RSC Adv. 9 (27) (2019) 15357–15369.
[36] A.K. Zak, M.E. Abrishami, W.A. Majid, R. Yousefi, S.M. Hosseini, Effects of annealing temperature on some structural and optical properties of ZnO nanoparticles prepared by a modified sol–gel combustion method, Ceram. Int. 37 (1) (2011) 393–398.
[37] M.A. Mousa, M. Khairy, Synthesis of nano-zinc oxide with different morphologies and its application on fabrics for U.V. protection and microbe-resistant defense clothing, Textil. Res. J. 90 (21–22) (2020) 2492–2503.
[38] S. Getie, A. Belay, A.R. Chandra Reddy, Z. Belay, Synthesis and characterizations of zinc oxide nanoparticles for antibacterial applications, J. Nanomed. Nanotechnol. S 8 (4) (2017).
[39] V. Dhiman, N. Kondal, P. Choudhary, Bryophyllum pinnatum leaf extract mediated ZnO nanoparticles with prodigious potential for solar-driven photocatalytic degradation of industrial contaminants, Environ. Res. 216 (2023) 114751.
[40] M. Golmohammadi, M. Honarmand, S. Ghanbari, A green approach to synthesizing ZnO nanoparticles using jujube fruit extract and their application in photocatalytic degradation of organic dyes, Spectrochim. Acta Mol. Biomol. Spectrosc. 229 (2020) 117961.
[41] A. Balcha, O.P. Yadav, T. Dey, Photocatalytic degradation of methylene blue dye by zinc oxide nanoparticles obtained from precipitation and sol-gel methods, Environ. Sci. Pollut. Control Ser. 23 (2016) 25485–25493. .
[42] B. Divya, C.H. Karthikeyan, M. Rajasimman, Chemical synthesis of zinc oxide nanoparticles and its application of dye decolourization, Int. J. Nanosci. Nanotechnol. 14 (2018) 267–275.
[43] S. Mondal, S.A. Ayon, M.S. Islam, M.S. Rana, M.M. Billah, Morphological evaluation and boosted photocatalytic activity of N-doped ZnO nanoparticles prepared via Co-precipitation method, Heliyon 9 (10) (2023) e20948. .
[44] M.F. Ramadan, A.T. Kareem, K. Al-Majdi, A.A. Omran, Exploration of zinc oxide nanoparticles for efficient photocatalytic removal of methylene blue dye: synthesis, characterization and optimization, Engineering Proceedings 59 (1) (2023) 120. .
[45] K.R. Ahammed, M. Ashaduzzaman, S.C. Paul, et al., Microwave assisted synthesis of zinc oxide (ZnO) nanoparticles in a noble approach: utilization for antibacterial and photocatalytic activity, SN Appl. Sci. 2 (2020) 955, https://doi.org/10.1007/s42452-020-2762-8.
[46] R.D. Wouters, P.C.L. Muraro, D.M. Druzian, A.R. Viana, E. de Oliveira Pinto, J.K.L. da Silva, W.L. da Silva, Zinc oxide nanoparticles: biosynthesis, characterization, biological activity and photocatalytic degradation for tartrazine yellow dye, J. Mol. Liq. 371 (2023) 121090. .

[47] D. Selvakumari, R. Deepa, V. Mahalakshmi, P. Subhashini, N. Lakshminarayan, Anti cancer activity of ZnO nanoparticles on MCF7 (breast cancer cell) and A549 (lung cancer cell), ARPN J. Eng. Appl. Sci. 10 (12) (2015) 5418–5421.
[48] R. Wahab, S. Dwivedi, A. Umar, S. Singh, I.H. Hwang, H.S. Shin, et al., ZnO nanoparticles induce oxidative stress in Cloudman S91 melanoma cancer cells, J. Biomed. Nanotechnol. 9 (3) (2013) 441–449, https://doi.org/10.1166/jbn.2013.1593 [PubMed ID: 23621000].
[49] S.H. Boskabadi, S.Z. Balanezhad, A. Neamati, M.H. Tabrizi, The green-synthesized zinc oxide nanoparticle as a novel natural apoptosis inducer in human breast (MCF7 and MDA-MB231) and colon (HT-29) cancer cells, Inorganic and Nano-Metal Chemistry 51 (5) (2020) 733–743. .
[50] A.Y. Aljohar, G. Muteeb, Q. Zia, S. Siddiqui, M. Aatif, M. Farhan, M.I. Ahamed, Anticancer effect of zinc oxide nanoparticles prepared by varying entry time of ion carriers against A431 skin cancer cells in vitro, Front. Chem. 10 (2022) 1069450. .
[51] G. Bisht, S. Rayamajhi, ZnO nanoparticles: a promising anticancer agent, Nanobiomedicine (Rij) 3 (2016) 9, https://doi.org/10.5772/63437.
[52] M. Zargarnezhad, S.N. Mirbahari, R. Ahmadi, The cytotoxic effects of zinc oxide nanoparticles on SW480 cell lines and measurement of nitric oxide in cell culture medium, Jentashapir Journal of Cellular and Molecular Biology 13 (1) (2022). .
[53] S.E. González, E. Bolaina-Lorenzo, J.J. Pérez-Trujillo, B.A. Puente-Urbina, O. Rodríguez-Fernández, A. Fonseca-García, R. Betancourt-Galindo, Antibacterial and anticancer activity of ZnO with different morphologies: a comparative study, 3 Biotech 11 (2021) 1–12. .
[54] V.V. Shinde, D.S. Dalavi, S.S. Mali, C.K. Hong, J.H. Kim, P.S. Patil, Surfactant free microwave assisted synthesis of ZnO microspheres: study of their antibacterial activity, Appl. Surf. Sci. 307 (2014) 495–502. .
[55] A.A. Tayel, W.F. EL-Tras, S. Moussa, A.F. EL-Baz, H. Mahrous, M.F. Salem, L. Brimer, Antibacterial action of zinc oxide nanoparticles against foodborne pathogens, J. Food Saf. 31 (2) (2011) 211–218.
[56] R.B. d'Água, R. Branquinho, M.P. Duarte, E. Maurício, A.L. Fernando, R. Martins, E. Fortunato, Efficient coverage of ZnO nanoparticles on cotton fibres for antibacterial finishing using a rapid and low cost in situ synthesis, New J. Chem. 42 (2) (2018) 1052–1060. .
[57] B. Lallo da Silva, M.P. Abuçafy, E. Berbel Manaia, J.A. Oshiro Junior, B.G. Chiari-Andréo, R.C.R. Pietro, L.A. Chiavacci, Relationship between structure and antimicrobial activity of zinc oxide nanoparticles: an overview, Int. J. Nanomed. (2019) 9395–9410.